Effect of surface morphology on the Ti–Ti adhesive bond performance of Ti6Al4V parts fabricated by selective laser melting

Ardila-Rodríguez, Laura Angélica; Rans, Calvin; Poulis, Johannes A.

DOI
10.1016/j.ijadhadh.2021.102918

Publication date
2021

Document Version
Final published version

Published in
International Journal of Adhesion and Adhesives

Citation (APA)
Ardila-Rodríguez, L. A., Rans, C., & Poulis, J. A. (2021). Effect of surface morphology on the Ti–Ti adhesive bond performance of Ti6Al4V parts fabricated by selective laser melting. *International Journal of Adhesion and Adhesives*, *110*, Article 102918. https://doi.org/10.1016/j.ijadhadh.2021.102918

International Journal of Adhesion & Adhesives 110 (2021) 102918

Contents lists available at ScienceDirect

International Journal of Adhesion and Adhesives

journal homepage: www.elsevier.com/locate/ijadhadh

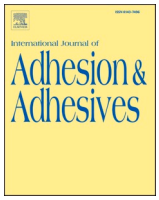

Effect of surface morphology on the Ti–Ti adhesive bond performance of Ti6Al4V parts fabricated by selective laser melting

Laura Angélica Ardila-Rodríguez *, Calvin Rans, Johannes A. Poulis

Structural Integrity, Faculty of Aerospace Engineering, Delft University of Technology, Delft, the Netherlands

ARTICLE INFO

Keywords:
Selective laser melting
Adhesive bonding
UV/Ozone treatment
Salt spray
Surface morphology

ABSTRACT

Surface morphology of adherends is an important factor to take into consideration when studying and improving the performance of an adhesive bonded joint. In this study, the adhesion performance three different surface morphologies of Selective Laser Melted (SLM) Ti6Al4V was studied. The three surface morphologies were created by manufacturing the adherends with different build directions (0, 45 and 90°). Scanning electron microscopy and laser confocal microscopy were used to assess the obtained morphology and roughness of the printed surface areas to be bonded. Those surfaces were subjected to 40 min of UV/Ozone treatment to remove organic contamination traces on the surface which lead to a reduced apparent contact angle and improved adhesive strength. The samples printed at 45°, which showed the highest surface roughness, presented the best adhesive performance during the tensile tests. The addition of sol-gel AC-120 and corrosion inhibition water-based primer BR 6747-1 showed an effective improvement in aging behaviour after 6 weeks of salt spray exposure.

1. Introduction

Surface preparation is well known to be a critical factor in the strength and durability of adhesive bonded joints. Many of these surface preparations focus on cleaning the surface of oxide layers and impurities to obtain a dry, grease-free and active surface. In addition to cleaning the surface, some surface preparation methods involve texturizing the surface by increasing its surface roughness. This can also increase adhesion performance as the modification of the surface roughness and morphology increases the net contact area and the potential for mechanical interlocking, meaning that the adhesive is locked into the irregularities of the substrate surface, traditionally shown as an "ink-bottle" shape [1,2]. Grit blasting and abrasion are texturizing methods commonly found in literature [1,3]. However, surfaces roughened by those pretreatment methods, usually do not show 'ink-bottle' like pits to enable mechanical interlocking as a major mechanism of adhesion. Instead, those texturizing methods positively influence the adhesive bond performance, as shown by Li et al. [4], ensuring that the substrates are free from organics, which aids subsequent wetting, creating a surface roughness that creates more area for interfacial contact. Laser surface texturizing is another technique that has been studied. Depending on the interaction between the laser process parameters and the material properties different surface textures can be generated modifying the chemistry and surface topography. Kurtovic et al. [5]. showed that the laser process leads to an increased surface roughness, wettability and adhesion properties. Nevertheless, to attain good adhesion strength, some other steps, besides surface texturizing, are necessary. Surface cleaning is an essential step in adhesive bonding in order to remove organic and inorganic contaminants from the surface. UV/Ozone treatment has been found to be a very effective cleaning technique in removing organic contaminations [6], as well as, atmospheric or vacuum pressure plasma [7]. Those cleaning treatments strongly reduces the consumption of chemicals and at the same time improve adhesion. In order to increase the durability of metallic adhesive bonds it is common practice to make use of chemical treatments such as chromic acid anodising [8] which by chemical dissolution of the metal and electrochemical oxidation of the surface creates a fresh well-defined oxide layer and a high degree of micro roughness to increase the surface area for physical and chemical bonding [9]. However, the use of strong chemicals is environmentally unfriendly as it requires a significant amount of energy, fresh water, special handling and disposal. In contrast, the use of sol–gel coatings, based on zirconium alkoxide and epoxy-silane, are treatments that show an excellent adhesive bond performance and durability, especially when used together with a water-based primer. The last one, is used to protect the bonded adherend from moisture attack and improve long-term durability. Aakkula et al. [10]. found that

* Corresponding author.
E-mail address: laardilar88@gmail.com (L.A. Ardila-Rodríguez).

https://doi.org/10.1016/j.ijadhadh.2021.102918
Received 19 February 2021; Received in revised form 29 April 2021; Accepted 22 May 2021
Available online 9 June 2021

grit blasting with sol-gel alone didn't provide durable adhesive bonding for titanium samples during hot/wet exposure. However, the results were acceptable when grit-blasting and sol-gel were followed with the application of BR 6747-1 chromate primer. Brack et al. [7]. studied the effect of mechanical and chemical treatments on titanium for bonding to a rubber toughened epoxy adhesive. Fracture energy measurements of wedge tests, exposed to 50 °C/95% relative humidity, showed that the addition of epoxy-silane treatment and BR6747-1primer treatments slowed the adhesive bond degradation rates and that the grit-blasting facilitated a higher initial fracture toughness.

In our previous research [11], titanium alloy surfaces were subjected to grit blasting treatments using UV/Ozone treatment. The results showed that the surface morphology and roughness increased with grit blasting pressure and the titanium was increasingly oxidized at longer UV/Ozone treatment times, leading to a reduced apparent contact angle and a better adhesive performance in a butt joint tension test. Furthermore, the addition of sol-gel AC-120 in combination with the BR 6747 primer showed an additional improvement in the initial adhesion after aging by exposure to salt-spray.

The aim of the present study is to revisit the outcomes of this study in a new context – that of adhesively bonding parts produced by the Selective Laser Melting (SLM) additive manufacturing process. The goal of grit blasting is to texturize the surface of a part to be bonded; however, inherent to the SLM process is the formation of a surface with an already high degree of surface roughness. This raises the question of how the surface morphology inherent to the SLM process compares to that of a traditionally grit blasted surface. Additive manufacturing (AM) easily allows the creation of complex geometries and internal features that are difficult or almost impossible to be processed by subtractive methods, and besides this reduces the processing steps and/or operations saving fabrication time [12]. Selective laser melting (SLM), a metal-based AM technique, uses a metal powder bed that is selectively scanned with a focused laser beam. The laser heat input causes a peak temperature that leads to a liquid phase formation (melting pool) by the melting of the powder particles. The amount of liquid phase formed depends on the amount of energy absorbed by the material, controlled by the laser power, the scanning speed, and the optical properties of the powder. Once the first layer is fully scanned, a new powder bed is disposed over the former and the process is repeated layer by layer until the part is completed. In the aerospace industry, fuel-saving and reduction of emissions are objectives that can be achieved by the use of more light-weight components for engines and structural parts. Through the research and application of additive manufacturing, those requirements could possibly be fulfilled. In 2015, GE Aviation began producing a 3D-printed fuel nozzle tip for the LEAP engine. By this technique, one single fuel nozzle tip was reduced from about 20 welded pieces to just one piece, leading to a weight reduction of about 25% [13].

The high stiffness of titanium together with the excellent corrosion resistance and good strength to weight ratio are some of the advantages that make titanium alloys useful in the transport industry. One of the applications of this material is the use as a repair patch material. Compared to composite patches, the material costs, the formability and time required to form a sheet of monolithic Ti repair patch to the desired shape are higher. However, additive manufacturing of titanium alloy to fabricate printed repair patches has been chosen as a strategy to save energy, time and thus costs by printing the patch directly at its final shape. This research focusses on the effect of the first step in the adhesive bonding process of the patch.

Typical surfaces of metal parts obtained by additive manufacturing observed on a micro-scale are rough and irregular. There are some causes of surface roughness such as the improper melting of powder particles, the "balling" effect, up-down skin and the "stair-step" effect. The improper melting of the powder particles could be a consequence of two production situations. One situation, exposed by DebRoy et al. [14], occurs when low heat input is used. The powder particles are not fully melted and stick to the surfaces of the build. Nguyen et al. [15]. observed the other situation when the dissipated heat from the molten pool at the focal point is enough, it can cause adjacent particles to be only partially melted and attach to the faces of the component. Another cause, described by Strano et al. [16], is the "balling" effect. Depending on the thermal variation across the melting pool, a surface tension gradient within the pool is created, and some material is pulled radially to the outer edges of the molten pool as small droplets that are located at the side edges of the track. Gravity is another condition that affects melt pools when created on unsupported layers, in this case described by Triantaphyllou et al. [17], the melted metal sticks to the unmelted powder below, resulting in a much rougher surface on the bottom part of the component (down skin) than on the upper surface (up skin). Finally, the surface roughness can be caused by a 'stair-step effect' which is the stepped approximation by layers of curves and inclined surfaces. In an ideal fabrication process of the layers, the surface texture will be a trigonometric function of the stepped geometry. However, in a real fabrication process, certain conditions in the melt pool, such as the three causes already mentioned above, will affect the shape of the layer edge which will result in deformations during the building process. Strano et al. [16], showed that the roughness obtained by this stair-step effect is a function of the layer thickness and the printing orientation angle.

Based on the above, the surface texturing step performed before the adhesive application to the adhesive repair patch could be avoided by taking advantage of the surface morphology and roughness obtained during the printing process. Nguyen et al. [15] investigated the adhesion properties of SLM titanium alloy (Ti–6Al–4V) surfaces in microscale, corresponding to the inherent roughness of the manufactured surfaces, and found that the "as-built" surface morphology can provide an increased contact area and mechanical interlocking between adhesive and adherend, which in turn maximises the adhesion potential of the adhesive. However, to the authors' knowledge, no more experimental studies have been reported on the bonding of AM surfaces in metal-metal joints. This paper aims at investigating the effect of the surface morphologies obtained in Ti6Al4V alloy parts, printed with three different orientations by SLM, the surface wetting and their adhesive bond performance in a butt-joint configuration. The durability of the adhesive bond after sol-gel and water-based primer application is also evaluated after aging in a salt spray chamber.

2. Methods

This adhesive bonding study was carried out using butt tension specimens fabricated by selective laser melting with three different printing orientations (0°, 45° and 90°) and consecutive either solvent and solvent together with UV/Ozone cleaning. The effectiveness of the obtained printed surfaces in relation to the cleaning treatment was quantified in two ways. First, the degree of surface cleaning was measured by contact angle measurements. Secondly, the samples were adhesively bonded and tension tests were performed. The durability of the bonded specimens, after applying sol-gel and primer, was investigated by a mechanical tension test after 6 weeks of salt-spray exposition and compared with specimens without aging. To aid in the discussion and evaluation of the obtained results, the test data were supplemented with surface morphology data, roughness measurements and fractography.

2.1. Specimen preparation

Specimens were produced on an Additive Industries MetalFAB1 machine using the standard parameter set for Ti–6Al–4V grade 23. Build preparation was made in Netfabb using a strip fill pattern and single contour. The powder used was supplied by Additive Industries to ASTM F3001 standard specification with a particle size range of 15–45 μm. The parts were manufactured in three batches of 50 parts with a support to reduce thermal distortions. Each batch comprised all the specimens of a single orientation. Heat treatment was performed at 920 °C for 2 h with

a heating rate of 10 °C/min and furnace cooling on each batch before removal from the build platform. Finally, the specimens were milled to reach the final dimensions and shape as presented Fig. 1a according to the ASTM standard D2094-00 (2014), but preserving the printed surface for the bonding process.

2.2. Surface preparation methods

The titanium specimens were cleaned by acetone and consecutively subjected to UV/Ozone treatment. The sol-gel and primer were applied to protect the surface within an hour after the UV/ozone treatment.

2.2.1. UV/ozone treatment

The UV/Ozone treatment was applied during 40 min using three low –pressure ozone generating mercury UV- light sources with a power of 30 Watt, (UV Technik, Germany) at a distance of 10 mm from the specimen's surface in a closed box. The UV/Ozone treatment time and distance were described in our previous research [11].

2.2.2. Sol-gel and primer application

To improve the stability of the obtained surface and to achieve an optimal adhesive bond between the metal and adhesive, AC-130-2 Sol-gel (3 M) and a water-based corrosion inhibiting primer BR 6747–1 (Solvay) were applied within an hour after the UV/Ozone treatment. The first one was applied by submerging the pre-bond surfaces for 2 min in the sol-gel. The surfaces were then dried for 30 min at room temperature and further cured at 60 °C for an additional 30 min. Finally, the BR 6747–1 primer was sprayed on top of the sol-gel using an air-atomizing gun within 1 h after the sol-gel application. The samples were again dried for 30 min, after which they were cured at 121 °C for 60 min.

2.3. Manufacturing process of adhesively bonded specimens

The adhesive bonding process was performed by applying the coin shaped film adhesive FM 94 K (Solvay, USA, nominal weight of 293 gsm, nominal thickness of 0.25 mm and polyester knit carrier) on the primer layer. The adhesive was cut with a stamp tube in rounded parts of 10 mm diameter. The film was placed between two titanium adherends previously prepared with the methods described in section 2.2. Subsequently, the adherends were aligned at 90° with the help of a pre-fabricated device suggested by ASTM D2094-00 and shown in Fig. 1b. A vacuum setup was arranged around the alignment device and the curing process was performed in an autoclave at 276 kPa pressure and 121 °C during 60 min with heating and cooling rates of 1 °C/min.

2.4. Test and measurement methods

The printed surfaces were studied in terms of obtained morphology, roughness and wettability, and the adhesively bonded samples were tensile tested, and the failure mode identified.

2.4.1. Surface roughness and morphology

Scanning Electron Microscopy (SEM) images of the surfaces of the printed specimens were acquired using a JEOL JSM 6010LA (JEOL, Tokyo, Japan) with Secondary Electrons detector (SE), 20.0 kV at a working distance of 10 mm. The surface roughness was measured by a Keyence Laser scanning Confocal Microscope VK-X3000 (Keyence International, Mechelen, Belgium) with a resolution of 1 nm. Each specimen's surface was measured at 3 different locations with an individual area of 60.000 μm^2. Of each orientation five specimens were tested and the average values and the standard deviations were obtained as the final result.

2.4.2. Contact angle

Contact angle measurements (CAM) were carried out using a Technex Cam200/Attension Theta V4.1.9.8 system (TECHNEX BV, Wormerveer, The Netherlands). The followed procedure is described in Section 10 of the ASTM D7490-13 [18] by curve fitting the profile of a 5 µl distilled water drop and measuring 6 times the angles formed between the tangents of the fitted curve and the horizontal axis. The averaged value of the measurements was taken as the result.

2.4.3. Tensile strength

A Zwick-Roell test machine (Zwick Roell Group) with a 10 kN load cell, was used to perform the butt tension tests, at room temperature and 55% RH, on five specimens per configuration following the ASTM standard D2095-96 (2015) [19]. A cardan was connected between the test machine (showed in Fig. 1c) and the grips to correct the axial alignment. The speed was 0.5 mm/min and the maximum load carried by the specimen at failure was recorded. The tensile strength was calculated by dividing the failure load by the area of the bonded surface. Both the arithmetic mean (averaged from the five repetitions per test) and the standard deviation are reported.

2.4.4. Fractography

The inspection of the fractured area on both adherends was measured using an enlargement of 25x on a Keyence VR-5000 wide-area 3D measurement system (Keyence International, Mechelen, Belgium). The remaining adhesive on the surfaces was measured using the Adobe Photoshop CC 2018 Color Range function and Equation (1) was used to calculate the percentage of remaining adhesive. The mean value and standard deviation was used for statistical analysis. Values closer to 100% are indicative of cohesive failure while values closer to 0% indicate more adhesive failure, values in between indicating a mixed-mode failure.

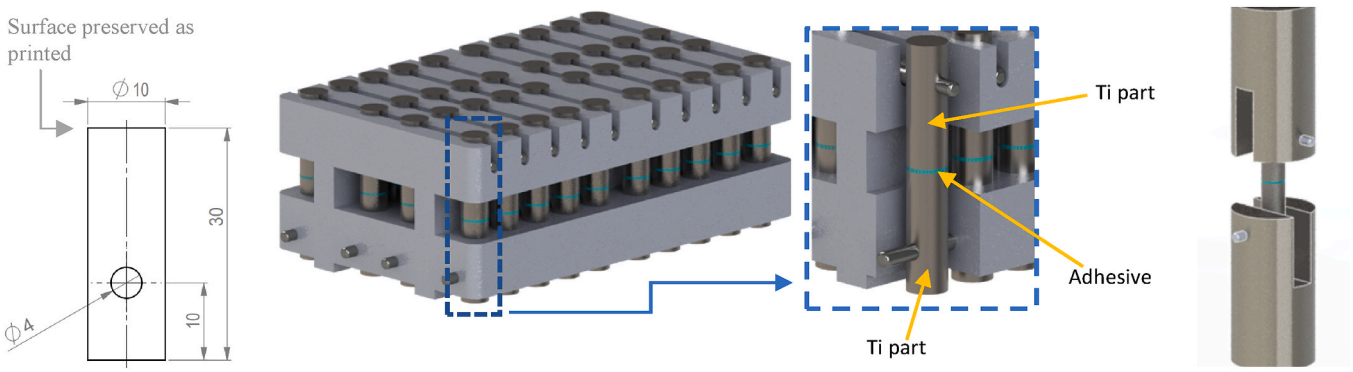

Fig. 1. (a) Titanium adherend with dimensions, (b) Alignment device showing in the section view of a bonded sample, (c) Tensile test setup.

$$\% \ of \ remaining \ adhesive = \left[\frac{remaining \ adhesive \ film \ area \ on \ both \ sides}{total \ bond \ area}\right] \times 100 \quad (1)$$

The sequence in which the methods, described in the previous sections, were used are summarized in Fig. 2.

2.4.5. Aging: salt spray exposure

The adhesively bonded specimens, UV/Ozone cleaned for 40 min and treated with sol-gel and primer for all three different printing orientations, were exposed to a neutral 5 wt% NaCl fog at 35 °C in a Liebisch Constamatic Salt Spray chamber (Gebr. Liebisch GmbH & Co. KG, Bielefeld, Germany) following the recommendations of the ASTM B117-18 standard [20] during 6 weeks (1000 h). The tensile strength and fractography, described in sections 2.4.3 and 2.4.4, were conducted on the samples before and after salt spray exposition.

2.4.6. Test matrix

A summary of the preparation methods applied and the names given to the specimens are presented in Table 1. All samples were pre-cleaned with acetone after the milling process and prior to the UV/Ozone cleaning. The first letter in the code is the indication of the printing orientation where *H* corresponds to the horizontal position (0° printing orientation), *A* to the angular orientation (45° printing orientation), and *V* to the vertical position (90° printing orientation). The number after the letter indicates the UV/Ozone cleaning time; 0 or 40 min. Thus specimens H0, A0 and V0 were only cleaned by acetone before being adhesively bonded. These samples are used for reference purposes. Finally, the capital letters SGP were used to identify the samples to which sol-gel AC-130-2 and primer BR 6747–1 were applied after being cleaned by acetone and 40 min UV/Ozone before being adhesively bonded. The grey-coloured background of Table 1 indicates the ageing period of 6 weeks in salt spray.

3. Results and discussion

3.1. Surface morphology and roughness

The surface roughness of the printed titanium parts was measured and Fig. 3 presents the roughness profile and a surface view together with the measured surface roughness parameter S_a (arithmetical mean height). Other surface roughness parameters such as Sz (maximum height), Sv (maximum pit height), Sp (maximum peak height) and Sq (root mean square height) were included in Table S1 of the Supplementary data. When the roughness parameter S_a presented in Fig. 3, is compared, it is observed that the roughness of the samples printed at 45° is the highest, closely followed by the roughness of the samples printed at 0°. However, the surface roughness of the samples printed at a 90° orientation is much less than the results found for samples printed at 0 and 45°. As observed in Fig. 3c, the roughness profile curve is smoother and the colour of the surface view image is more homogeneous compared to the samples printed at 0 and 45° (Fig. 3a and b). The changes in the surface roughness values are dominated by the presence of balls formed during the printing process over the three types of samples which are certainly more evident in the samples printed at 0 and 45° but are still present in a lower amount in the sample printed at 90°. This implies that the printing orientation has a significant influence on the surface morphology and roughness. As the printing orientation changes from 0 to 45°, an increase in the number of the balls is found, and, as a consequence, an increase in the surface roughness. In contrast, at the surface of the samples printed at 45 and 90°, a huge reduction in surface roughness and number of balls is present.

Fig. 4 shows the SEM images of the surface of the samples in which different surface morphologies are observed. The first clear observation is that in Fig. 4a and c the scanning patterns (highlighted by lines) are evident, while in Fig. 4b it is masked in some extent by the presence of balls and ridges on the surface. In Fig. 4a, the background of the surface looks smooth but the surface roughness results from the presence of

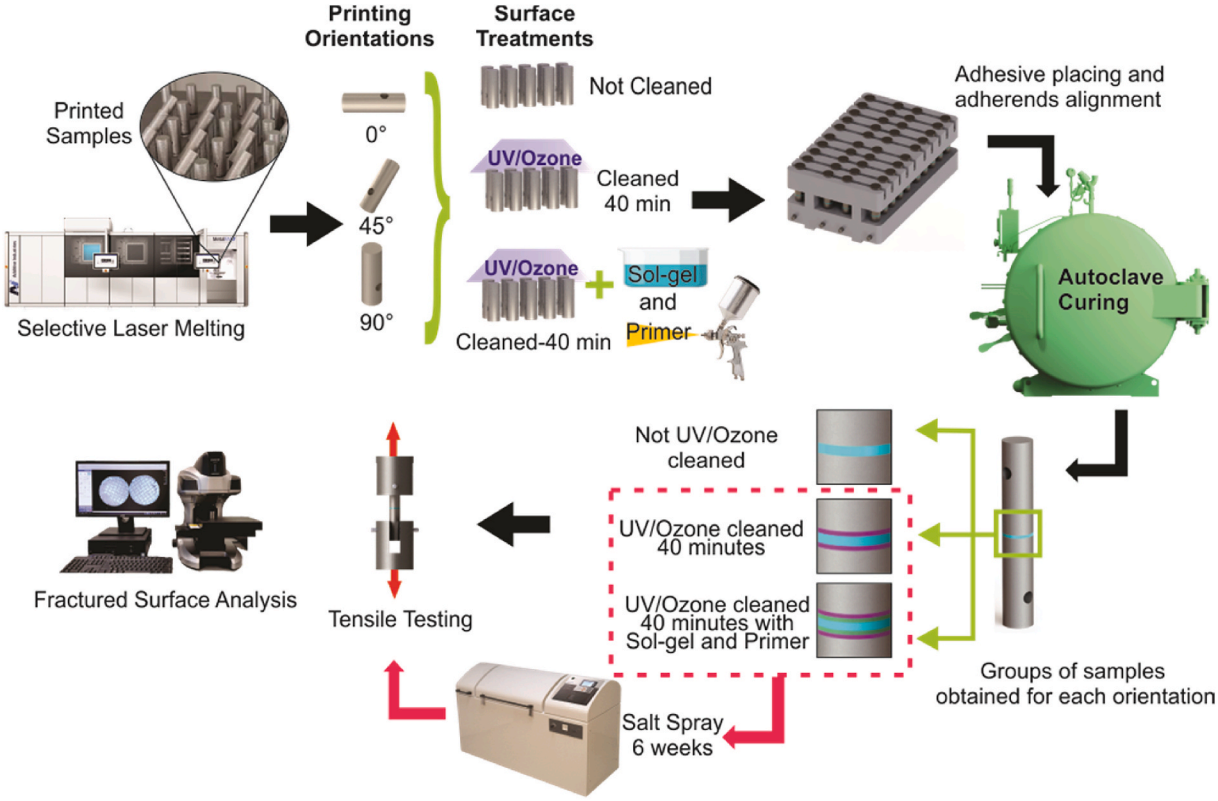

Fig. 2. The sequence followed for the preparation and characterization of the specimens.

Table 1
Specimens' description.

Parameters	Specimen								
	H0	H40	HSGP	A0	A40	ASGP	V0	V40	VSGP
Printing Orientation (°)	0	0	0	45	45	45	90	90	90
UV/Ozone Time (min.)	0	40	40	0	40	40	0	40	40
Sol-Gel AC-130–2 and Primer BR 6747–1			✓			✓			✓

Samples grey-coloured were exposed to 6 weeks of Salt Spray.

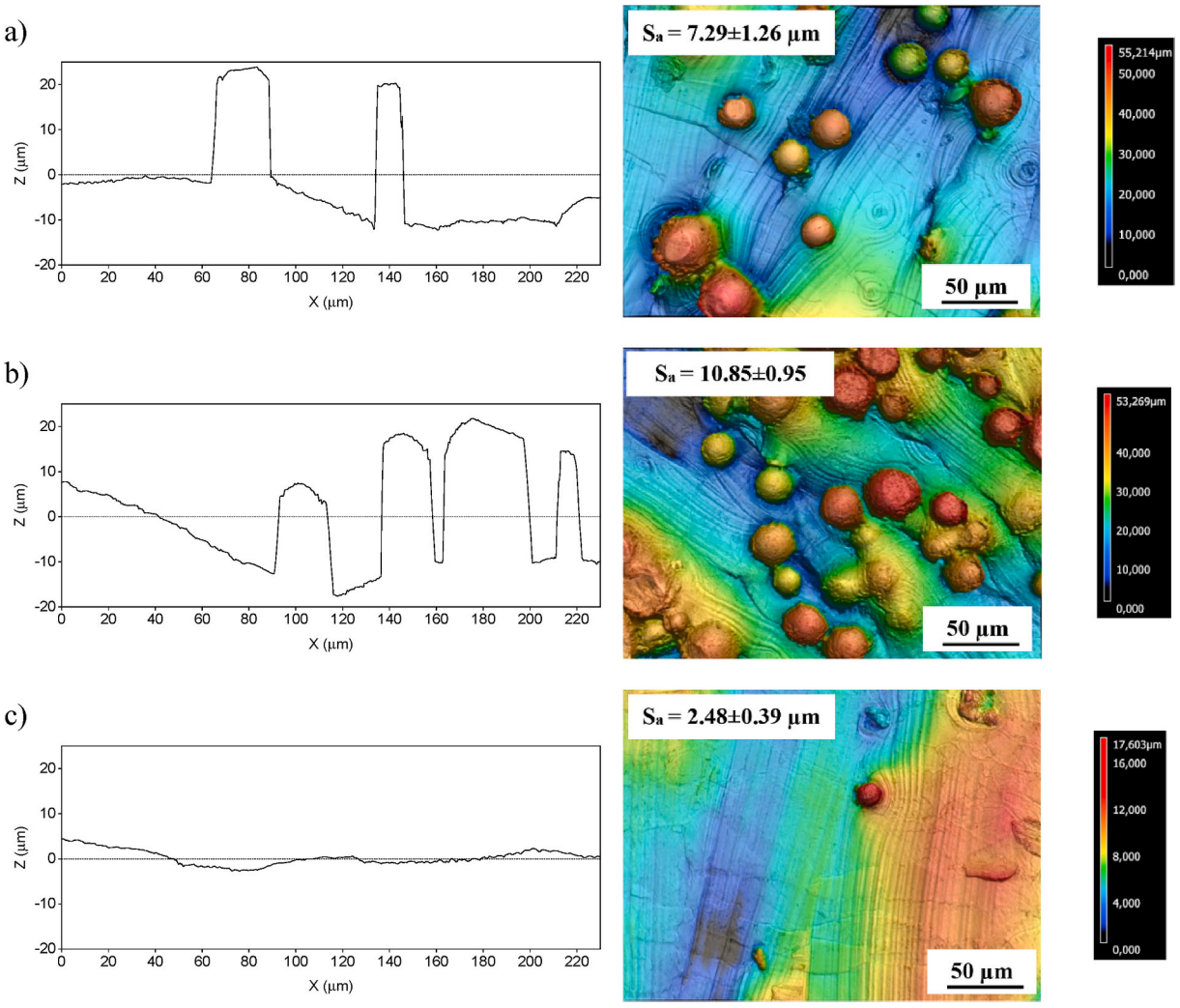

Fig. 3. Roughness profile in which Z is the average roughness height and X the sampling length (left) and surface view of Ti6Al4V printed with (a) 0°, (b) 45° and (c) 90° orientation.

some particles on the edge of each scanned layer. The same characteristic was observed in Fig. 4c but with a lower quantity and size of scattered particles on the edge of some scanning tracks. In Fig. 4b, parallel ridges with high waviness are observed on the surface with partially bonded particles stuck at the edges of the layers with the highest size of the particles found in all printing orientations.

Surface quality in selective laser melted parts is usually characterized by the presence of the "balling" effect caused by the rupture of the melting pool into small spherical particles that are scattered on both sides of the pool or the scanned track. Strano et al. [16]. showed that these are almost completely removed when the next track is scanned. This is clearly the case when the sample printed at 90° (Fig. 4f) is considered. Another effect that affects the surface of a printed part, described by the same author, is that the partially bonded particles are stuck at the steps (or layer edges). The cause is that the heat of the edge borders is not enough to fully sinter the particles. As a result, the particles do not merge completely within the printing layer and tend to stick to the surface at the step edges. This is the case with the samples printed at 0° (Figure 4d) and 45°. However, at the samples printed at 45°, the stair-step influences the surface morphology once those attached particles fill the spaces between the edges or layers that are closer to each other, thus causing waviness and parallel ridges (Fig. 4e).

3.2. Contact angle measurements

The static apparent contact angle values summarized in Fig. 5 show the modification of the titanium surfaces obtained by different printing orientations cleaned with acetone and following UV/ozone cleaning.

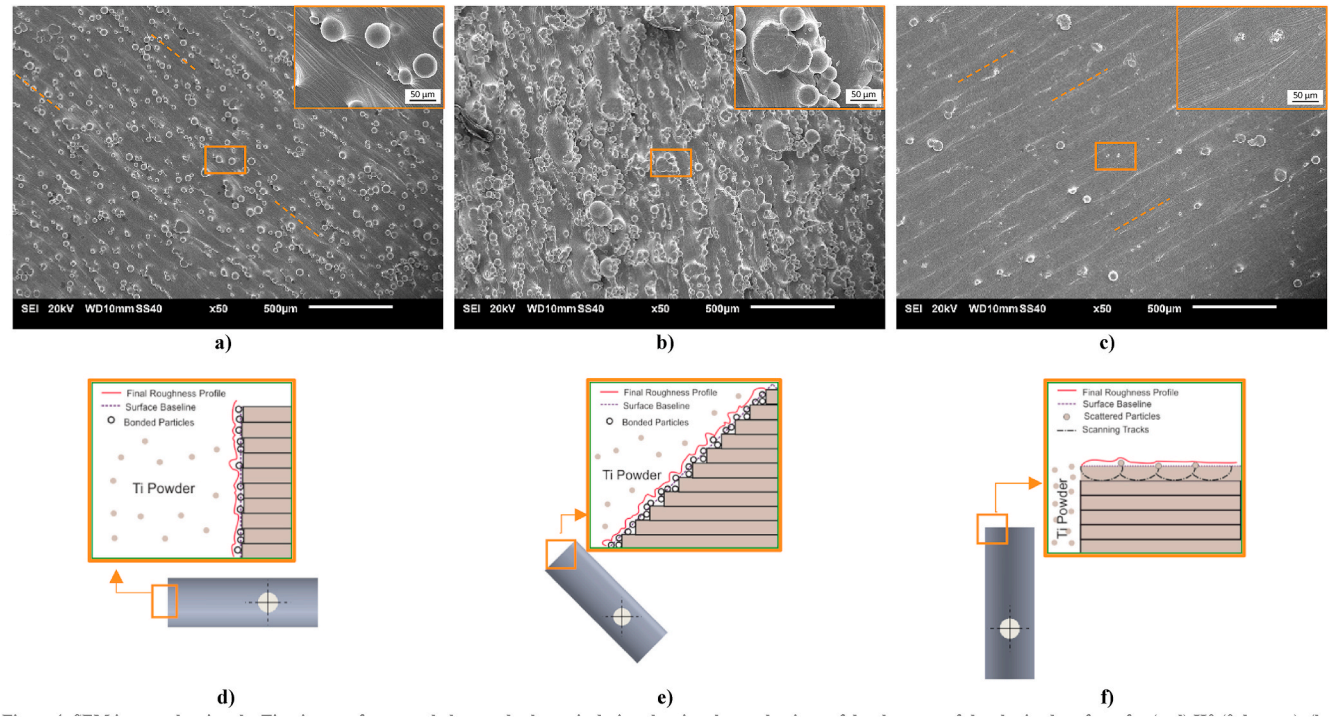

Fig. 4. SEM images showing the Titanium surface morphology and schematic design showing the mechanisms of development of the obtained surfaces for (a, d) H0 (0°), (b, e) A0 (45°) and (c, f) V0 (90°). The scanning patterns are highlighted by lines.

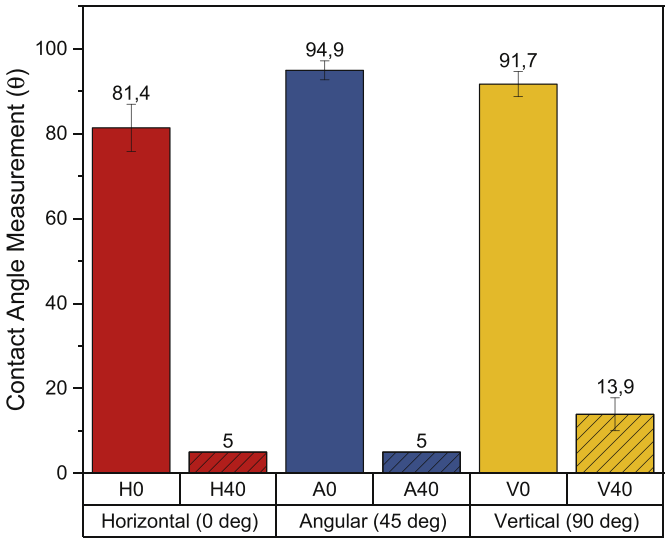

Fig. 5. Contact angle measurements for the different printing orientations cleaned with acetone (H0, A0, V0) and those cleaned with acetone as well as 40 min of UV/Ozone exposure (H40, A40, V40).

When the surfaces of the three different printing orientations were just cleaned with acetone, which is expected to remove most organic contaminations, the sample printed at 0° (H0) shows the lowest contact angle value of 81.4° followed by the sample printed at 90° (V0) with 91.7° and finishing with the sample printed 45° (A0) with 94.4°. As showed in the previous section, the sample H0 obtained a medium value of surface roughness of about 7 μm and its surface morphology shows small melted particles distributed homogeneously all over its surface. This sample has the lowest apparent contact angle. At sample V0, a low roughness of about 2.5 μm and flat surfaces with some ripples but limited melted particles were observed which reduce the surface area and limits wetting. However, this sample has the second lower apparent contact angle. The A0 samples show a ridge waviness morphology with the higher surface roughness of about 11 μm and the highest apparent contact angle within the three orientations when just cleaned with acetone. The change in the apparent contact angle, as was shown by Wenzel [21], is related to the roughness factor. Roughening the surface increases the apparent surface free energy and consequently the extent of wetting. However, the results observed in this group of samples do not seem to conform to that regime, samples A0 show the highest roughness but also the highest value of the apparent contact angle. That performance could be explained by the sharp protrusions observed on samples A0, which may have limited the acetone cleaning, leaving a mono layer of surface contaminations between the valleys of the roughness, reducing the wetting. Those protrusions might also prevent the adhesive from fully penetrating into the ridges, as showed by Li et al. [4]. At this point it is worth mentioning that the surface morphology plays a significant role and should be understood to take advantage of, otherwise it could be detrimental for the final results. Besides this, the surface roughness alone is not enough to acknowledge for a low apparent contact angle, or even a good adhesive performance, it must always go together with a high degree of cleaning and should preferably be accompanied by modifications in the surface chemistry.

When samples were cleaned during 40 min by UV/ozone, the apparent contact angle values follow Wenzel's statement, and are reduced to less than 5° for the samples printed at 0° (H40) and 45° (A40) and to 13.9° for the samples printed 90° (V40). The general reduction, following the discussion presented in the previous paragraph, is a consequence of the improved removal of the last traces of organic contaminations [22], even in the valleys of the surface, followed by changes in the surface oxide composition induced by the UV/Ozone treatment due to titanium oxidation as shown in our previous work [11].

3.3. Initial adhesive bond performance

The adhesive bond performance of the group of samples which were cleaned by acetone in combination with 40 min of UV/Ozone and pre-

treated with sol-gel and primer are presented in Table 1. They were accessed by mechanical tests.

The tensile strength of the tested bonded joints are summarized in Fig. 6a. The failure surfaces were evaluated and the results of the calculations obtained from Equation (1) are summarized in Fig. 6b. The photographs of the failure surfaces are presented in Fig. 7.

It can be seen that there was a difference in the tensile strength between the three printing orientations after cleaning with acetone (see trend plots in Fig. S1). Those results are in line with the apparent contact angle measurements discussed in the previous section. As observed in the corresponding photographs in Fig. 7, these groups of samples showed a relatively high adhesive type of failure mode, shown by the lacking adhesive at the counterpart areas. Sample H0, printed at 0°, which presents a medium surface roughness with the lowest apparent contact angle value, showed the highest tensile strength (41.2 MPa) and percentage of remaining adhesive (57.1%) respectively. This was followed by the sample V0, which has the lowest roughness value, with a tensile strength of 33.9 MPa and a percentage of remaining adhesive of 54%. Sample A0 shows the higher roughness and an apparent contact angle value with a tensile strength of 25.6 MPa and a percentage of remaining adhesive of 52.4%. These results show that the samples with

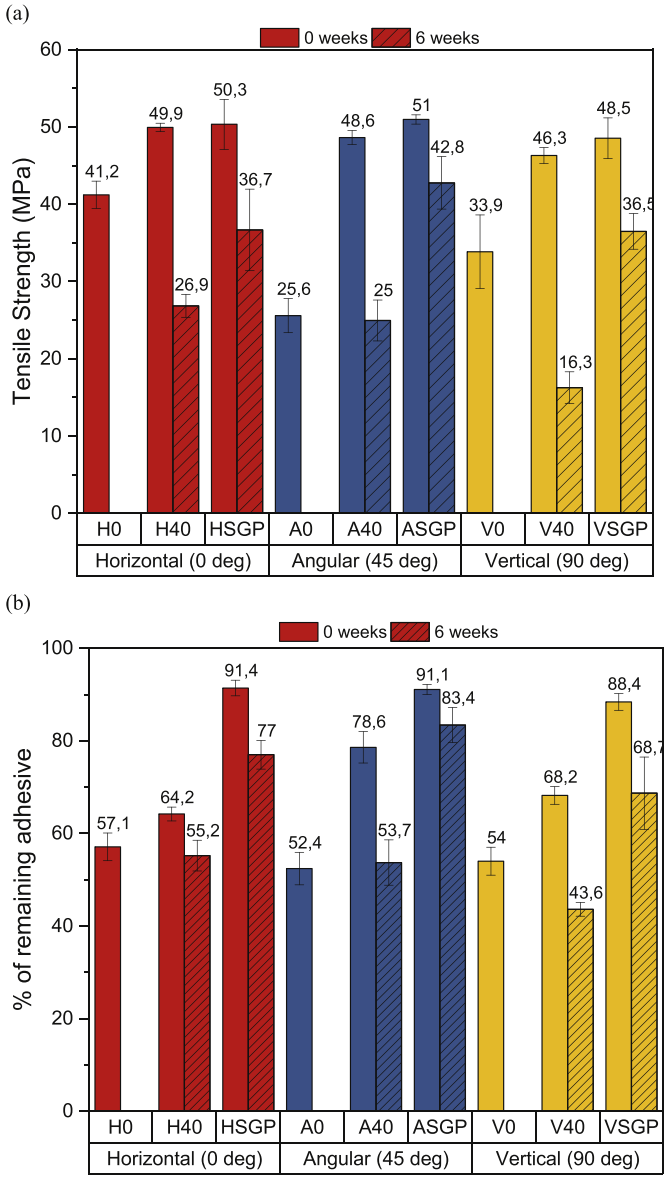

Fig. 6. (a) Tensile strength, (b) percentage of remaining adhesive.

the lower apparent contact angle values presented a better adhesive joint performance due to increased wetting. However, as discussed in Section 3.1, samples printed at 45° show a higher surface roughness and more prominent surface morphology, which could indicate a good adhesive performance. Nevertheless, its topography could also cause difficulties to obtain good cleaning performance with acetone only. This causes not just a high apparent contact angle value, but also more adhesive failure and the poorest tensile strength observed in this work and described by Petrie [3] as a consequence of internal stress concentrations caused by trapped gas, voids or inclusions, due to bad surface wetting. On the other hand, samples printed at 90° showed the lowest roughness indicating a limited contact area between the adherend and the adhesive and less possibility of interlocking.

After 40 min of UV/Ozone cleaning the comparison between the samples continue to follow the results obtained from apparent contact angle measurements in which samples printed at 0° (H40) and 45° (A40) obtained the lower apparent contact angle value (less than 5°). As observed in the corresponding photographs in Fig. 7, this group of samples showed a mixed failure mode with areas where the layer of adhesive remains on both adherend surfaces, which indicates a cohesive failure, together with some other areas showing adhesive failure. Within this group of samples, the ones printed at 45° reach a higher cohesive failure mode with at best a remaining adhesive value of 78.6% and a tensile strength of 48.6 MPa. Samples printed at 0° (H40) show a comparable tensile strength of 49.9 MPa within the standard deviation and a lower percentage of remaining adhesive of 64.2%. Finally, samples printed at 90° (V40) with the higher contact angle value reached the lowest tensile strength of 46.3 MPa and a percentage 68.2% of remaining adhesive, close to that obtained for the sample H40. As previously suggested, the organic traces that were supposed to remain on the samples printed at 45° after acetone cleaning (A0), were removed after cleaning with UV/Ozone (A40). The enhanced cleaning effect leads to improved tensile strength values that are in line with the apparent contact angle data and roughness (See Fig. S1). Showing that the surface cleaning and chemistry are important and sensitive steps to succeed in a good adhesive bond performance.

The samples to which sol-gel AC-130-2 and the BR 6747–1 primer were applied (HSGP, ASGP and VSGP) presented the best performance, of all the samples studied in this research, with cohesive failure as the dominant failure mode with small areas of adhesive failure as shown in Fig. 7. The samples printed at 45° show the highest average values of tensile strength and percentage of remaining adhesive.

3.4. Aging: salt spray

Test samples (see Table 1) were exposed to salt spray fog during 6 weeks (1000 h) to determine the durability of the adhesive joints. The results obtained before and after the 6 weeks are compared in Figs. 6 and 7.

As a general observation of Fig. 6a, it can be concluded that the samples without aging (0 weeks) show a higher tensile strength than the aged ones. After 6 weeks of aging, there is a huge reduction of the average tensile strength within the standard deviation, for the samples just cleaned with 40 min UV/Ozone. Amongst them, samples H40 and A40 showed similar average values that drops to almost 54% of its non-aged value, and sample V40 presented a more severe reduction and drops to almost 41% of its initial non-aged value.

The tensile strength values obtained from the samples treated with sol-gel and primer treatment show a much less severe reduction. After 6 weeks, the tensile strength of the samples HSGP and VSGP were similar within the standard deviation and reduce to roughly 75% of its initial non-aged value, and the tensile strength of the sample ASGP, which presents the best performance, still preserves 84% of its initial non-aged value.

The results of calculated percentages of remaining adhesive for samples just cleaned by UV/Ozone H40, A40, and V40, observed in

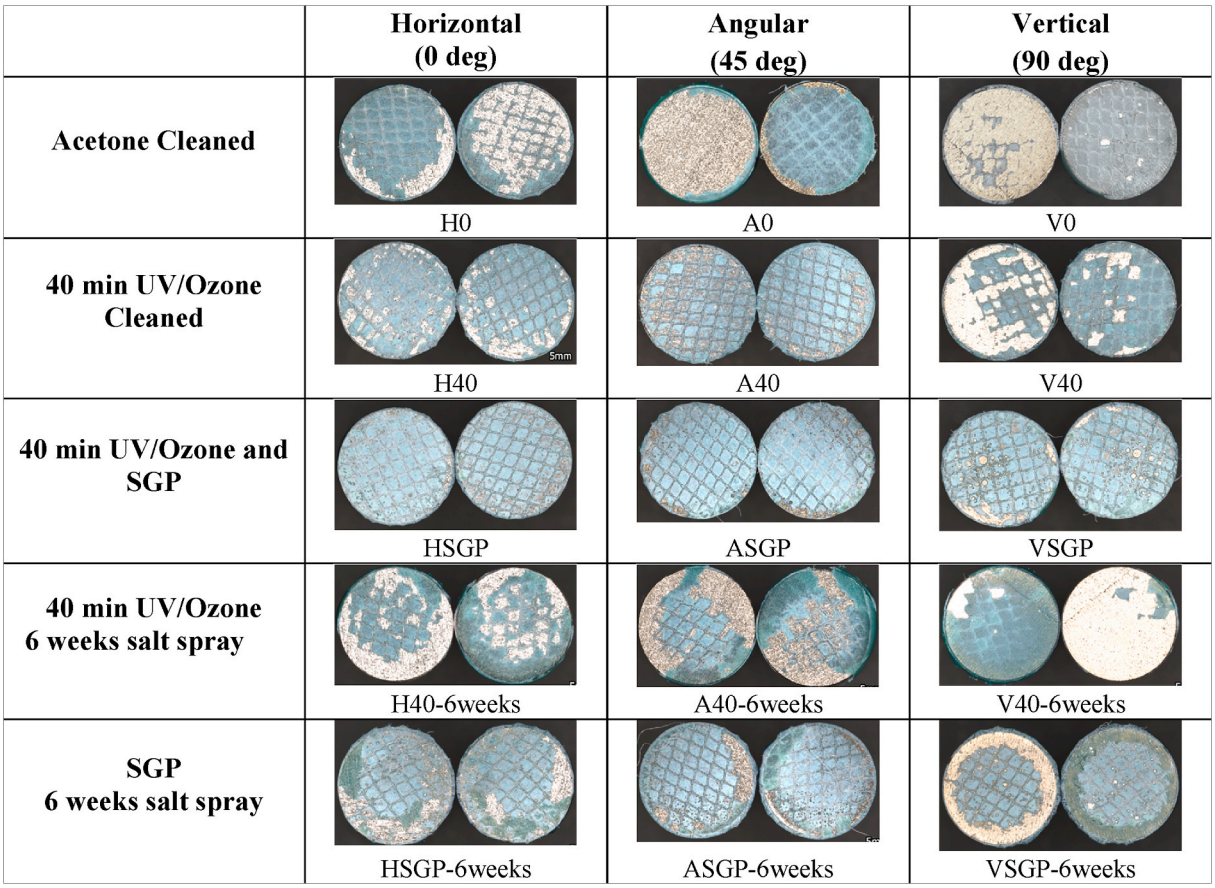

Fig. 7. Fractured surfaces after 0 and 6 weeks of salt spray exposure.

Fig. 6b, were reduced from 64%, 79%, and 68%–55%, 54%, and 44%, respectively after salt spray. In line with those results are the fractography images presented in Fig. 7, where the change from mixed cohesive failure to adhesive failure at the interface after the salt spray exposure is observed. Moisture penetration on the interface, possibly by the hydration of the thickened oxide layer developed in the titanium alloy surface after the UV/Ozone cleaning [11], leads to the depletion, plasticization and swelling of the adhesive, which is eventually displaced from the substrate resulting in adhesive failure and the reduction in the tensile strength. Park et al. [23]. observed this behaviour as a result of hydration of the anodic oxide layer obtained by phosphoric acid containment systems (PACs). The observed interfacial failure was expected rather than corrosion since the Ti6Al4V alloy has an excellent corrosion resistance. Studies of Li et al. [24]. and Ciszak et al. [25]. have shown the effect of NaCl on the surface of Titanium alloy has only shown proof of corrosion on the surface when performed at temperatures above 400 °C (see Fig. S2). In contrast, the samples with sol-gel and primer, show a cohesive failure as the dominant failure mode with only small areas of adhesive failure and calculated percentages of remaining adhesive of 91%, 91%, and 88% for the samples HSGP, ASGP, and VSGP, respectively. Those calculated percentages of remaining adhesive values are reduced to 77%, 83%, and 68%, respectively with the increase of the adhesive failure areas after 6 weeks of aging. This group of samples thus presented a durable adhesive bond after 6 weeks of exposure time with mostly cohesive failure due to, on the one hand, the two principal components of the sol-gel, the organosilane that promotes superior bonding, and the zirconium that creates a strong covalent bond with the adherend and acts as an oxygen diffusion barrier [26] and, on the other hand, the water-based epoxy primer ensure the coupling between the sol-gel and the epoxy adhesive, thus enhancing the durability of the adhesive bond. Aakkula et al. [10]. found to be necessary the use of BR 6747–1 water-based primer for durable adhesion in titanium and stainless steel bonds after the sol-gel application.

In our previous work [11], the best conditions found to prepare the Ti6Al4V specimens were grit blasting with 5 bar of pressure, obtaining a surface roughness Sa of about 2 μm (see Table S1). UV/Ozone cleaning during 40 min in combination with sol-gel AC-130-2 and with BR 6747–1 primer were applied and samples were exposed to salt spray aging. By analysing the best results of that research and comparing them in Fig. 8 with the best results found in the present work, which corresponds to the samples printed at 45°, it becomes possible to appreciate that the samples printed 45°, returned the same results of tensile strength and percentage of remaining adhesive as was obtained by the surface texturing with grit blasting. However, it is worth noticing, that the roughness value of the grit blasted surface is much lower than that of the roughness obtained by 3D printing at 45°. Almost the same value of roughness was obtained for the sample printed at 90°, which presented the poorest results throughout this research.

That is why the performance of the bonded surfaces should be analysed in the whole context. Both samples, grit-blasted and 90° printed have almost the same roughness but a completely different surface morphology, being the grit-blasted prominent with elevations and valleys while the 90° printed one is smooth and homogeneous with some small spherical particles scattered (See Fig. S3). That is completely opposite to the surface morphology of the 45° printed samples, which show parallel ridges with high waviness, partially bonded high sized particles and a roughness of about 11 μm (Fig. 3b). In this specific comparison, the difference in performance of the grit blasted samples and the samples printed at 45° is attributed probably to the surface morphology that allows an increased surface area for bonding more than to the surface roughness.

The last results present the possibility of saving time (and costs) by

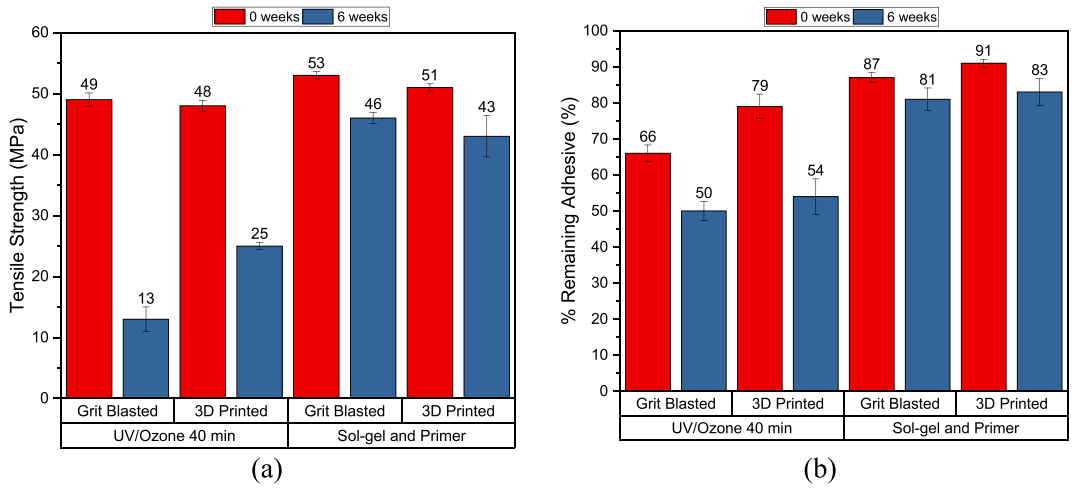

Fig. 8. Comparison of (a) Tensile strength and (b) the percentage of remaining adhesive, between 3D printed samples evaluated in the present work and grit blasted bulk titanium.

avoiding a regularly used (but often shape-deforming) conventional pretreatment step such as grit blasting. The cost savings of printing a repair patch directly in its final three-dimensional shape instead of the conventional forming process is also an advantage. However, is still necessary to study the fatigue durability and other mechanical properties of the additive manufactured printed titanium and assess whether it satisfies the conditions to be used as a repair patch material in aircraft repairs.

4. Conclusion

In this work, experiments were conducted to analyse the effect of both the printing orientation and the UV/Ozone cleaning of Ti6Al4V selective laser melted specimens in their adhesive behaviour by tensile tests and fractography. The effectiveness of UV/ozone cleaning in combination with sol-gel and a modified water-based epoxy primer on the durability of the adhesive bonds exposed to salt spray were studied. Based on these results, conclusions can be summarized as follows:

1. The printed samples surface morphology changed with the printing orientation, with the stair-step effect showing a major increase in surface roughness.
2. The printed titanium surfaces which were only cleaned by acetone didn't show an effective cleaning effect when the roughest topography was considered. After UV/ozone treatment all the studied printed orientations showed a substantial reduction in the apparent contact angle, which is most probably due to the removal of the remaining traces of organic contamination, especially in the valleys of the surface's roughness.
3. The adhesive performance was in line with the apparent contact angle measurement results and was higher at the samples with higher surface roughness but just after being cleaned by UV/Ozone, showing the effectiveness of UV/Ozone as a cleaning surface treatment.
4. The samples with sol-gel and primer showed improved aging behaviour with mostly cohesive failure.
5. The bonding potential of additive manufactured surfaces in metal-metal joints was established but further studies are necessary to make this approach fully applicable as a repair patch material in aerospace industry.

Acknowledgements

This project is part of Work package 4 of the project 'Fieldlab Composieten Onderhoud & Reparatie: bouwen aan het DCMC' of the 1.B.1 innovation program OP Zuid 2014–2020 which is subsidized by the European Union and supported by the Provincie Noord-Brabant, of The Netherlands.

This research was supported by the Fraunhofer Project Center at the Universiteit Twente (FPC@UT).

Furthermore, the authors would like to thank Cees Paalvast for applying primer and sol-gel, and all the staff of the Delft Aerospace Structures and Materials Laboratory and the DEMO University workshop for their collaboration during the realization of this project.

Appendix A. Supplementary data

Supplementary data to this article can be found online at https://doi.org/10.1016/j.ijadhadh.2021.102918.

References

[1] Kinloch AJ. Adhesion and adhesives: science and technology. Chapman & Hall; 1987. https://doi.org/10.3131/jvsj.9.5.
[2] da Silva LFM, Ochsner A, Adams RD, editors. Handbook of adhesion technology, vols. 1–2. Berlin, Heidelberg: Springer; 2011. https://doi.org/10.1007/978-3-319-55411-2_8.
[3] Petrie EM. Handbook of adhesives and sealants. McGraw-Hill Education; 2007.
[4] Li J, Li Y, Huang M, Xiang Y, Liao Y. Improvement of aluminum lithium alloy adhesion performance based on sandblasting techniques. Int J Adhesion Adhes 2018;84:307–16. https://doi.org/10.1016/j.ijadhadh.2018.04.007.
[5] Kurtovic A, Brandl E, Mertens T, Maier HJ. Laser induced surface nano-structuring of Ti-6Al-4V for adhesive bonding. Int J Adhesion Adhes 2013;45:112–7. https://doi.org/10.1016/j.ijadhadh.2013.05.004.
[6] Yasuda K, Okazaki Y, Abe Y, Tsuga K. Effective UV/Ozone irradiation method for decontamination of hydroxyapatite surfaces. Heliyon 2017;3:e00372. https://doi.org/10.1016/j.heliyon.2017.e00372.
[7] Brack N, Rider AN. The influence of mechanical and chemical treatments on the environmental resistance of epoxy adhesive bonds to titanium. Int J Adhesion Adhes 2014;48:20–7. https://doi.org/10.1016/j.ijadhadh.2013.09.012.
[8] Kwakernaak A, Hofstede J, Poulis J, Benedictus R. Improvements in bonding metals (steel, aluminium). Adv. Struct. Adhes. Bond. Elsevier Science; 2010. p. 185–236.
[9] Callinan RJ, Galea SC. Advances in the bonded composite repair of metallic aircraft structure. https://doi.org/10.1016/B978-008042699-0/50021-8; 2002. 2.
[10] Aakkula J, Saarela O. Silane based field level surface treatment methods for aluminium, titanium and steel bonding. Int J Adhesion Adhes 2014;48:268–79. https://doi.org/10.1016/j.ijadhadh.2013.09.039.
[11] Ardila-Rodríguez LA, Boshuizen B, Rans C, Poulis JA. The influence of grit blasting and UV/Ozone treatments on Ti-Ti adhesive bonds and their durability after sol-gel and primer application. Int J Adhesion Adhes 2021;104:102750. https://doi.org/10.1016/j.ijadhadh.2020.102750.
[12] Ian Gibson IG. Introduction and basic principles. Addit. Manuf. Technol. 3D printing, rapid prototyping, direct digit. Manuf. Springer; 2015. p. 1–18.
[13] General Electric. New manufacturing milestone: 30,000 additive fuel nozzles. GE Addit; 2018. https://www.ge.com/additive/stories/new-manufacturing-milest

one-30000-additive-fuel-nozzles%0Ahttps://www.ge.com/additive/blog/new-manufacturing-milestone-30000-additive-fuel-nozzles.
[14] DebRoy T, Wei HL, Zuback JS, Mukherjee T, Elmer JW, Jo Milewski, et al. Additive manufacturing of metallic components – process, structure and properties. Prog Mater Sci 2018;92:112–224. https://doi.org/10.1016/j.pmatsci.2017.10.001.
[15] Nguyen ATT, Brandt M, Orifici AC, Feih S. Hierarchical surface features for improved bonding and fracture toughness of metal-metal and metal-composite bonded joints. Int J Adhesion Adhes 2016;66:81–92. https://doi.org/10.1016/j.ijadhadh.2015.12.005.
[16] Strano G, Hao L, Everson RM, Evans KE. Surface roughness analysis, modelling and prediction in selective laser melting. J Mater Process Technol 2013;213:589–97. https://doi.org/10.1016/j.jmatprotec.2012.11.011.
[17] Triantaphyllou A, Giusca CL, MacAualy GD, Leach RK, Milne K a. Surface texture measurement for additive manufacture. Proc ASPE Spring Top Meet Dimens Accuracy Surf Finish Addative Manuf 2014;3:127–30. https://doi.org/10.1088/2051-672X/3/2/024002.
[18] ASTM. Standard D7490-13: standard test method for measurement of the surface tension of solid coatings, substrates and pigments using contact angle measurements. ASTM Int 2013:1–5. https://doi.org/10.1520/D7490-13.2.
[19] ASTM. Standard D295-96. Standard test method for tensile strength of adhesives by means of bar and rod specimens. ASTM Int 2015; 2015. https://doi.org/10.1520/D2095-96R15.2.
[20] ASTM. Standard B117: standard practice for operating salt spray (fog). ASTM Int; 2011. https://doi.org/10.1520/B0117-11.2.
[21] Wenzel RN. Resistance of solid surfaces to wetting by water. Ind Eng Chem 1936;28:988–94. https://doi.org/10.1021/ie50320a024.
[22] Kohli R. Applications of UV-ozone cleaning technique for removal of surface contaminants, vol. 11. Elsevier Inc.; 2019. https://doi.org/10.1016/b978-0-12-815577-6.00009-8.
[23] Park SY, Choi WJ. Investigation on the effectiveness of silane-based field level surface treatments of aluminum substrates for on-aircraft bonded repairs. Int J Adhesion Adhes 2019;95:102414. https://doi.org/10.1016/j.ijadhadh.2019.102414.
[24] Li R, Wang S, Zhou D, Pu J, Yu M, Guo W. A new insight into the NaCl-induced hot corrosion mechanism of TiN coatings at 500 ° C. Corrosion Sci 2020;174:108794. https://doi.org/10.1016/j.corsci.2020.108794.
[25] Ciszak C, Popa I, Brossard J, Monceau D, Chevalier S. NaCl induced corrosion of Ti-6Al-4V alloy at high temperature. Eval Progr Plann 2016;110:91–104. https://doi.org/10.1016/j.corsci.2016.04.016.
[26] Blohowiak Kay Y, Osborne Joseph H, Krienke KA. Sol for coating metals. 1998.